Biocontrol Science, 2022, Vol. 27, No. 4, 217－222

Note

Remote Bactericidal Effect of Anatase TiO_2 Photocatalytic Nanoparticles Annealed with Low-Temperature O_2 Plasma

RETSUO KAWAKAMI[1]*, YUKI TAKAO[1], AKIHIRO SHIRAI[2], AND TAKASHI MUKAI[3]

[1]*Department of Science and Engineering, Graduate School of Technology, Industrial and Social Sciences, Tokushima University, 2-1 Minami-Josanjima, Tokushima 770-8506, Japan*
[2]*Department of Bioscience and Bioindustry, Graduate School of Technology, Industrial and Social Sciences, Tokushima University, 2-1 Minami-Josanjima, Tokushima 770-8513, Japan*
[3]*Nichia Corporation, Anan, Tokushima 774-0044, Japan*

Received 10 May, 2022/Accepted 10 July, 2022

The remote bactericidal effect of TiO_2 photocatalyst, i.e., the bactericidal effect away from the photocatalyst, was successfully achieved using a humidified airflow. The TiO_2 photocatalyst used was anatase-type TiO_2 nanoparticles (NPs) annealed with a low-temperature O_2 plasma. For comparison, anatase-type TiO_2 NPs annealed in the air were used. The bacteria, *Bacillus subtilis*, were placed away from the TiO_2 NPs. The plasma-assisted-annealed TiO_2 NPs significantly inactivated 99% of the bacterial cells in 5 h, whereas the pristine and air-annealed TiO_2 NPs inactivated 88-90% of the bacterial cells. The remote bactericidal effect of plasma-assisted-annealed TiO_2 NPs would be attributed to a larger amount of H_2O_2 molecules traveled by the airflow from the TiO_2 NPs. The molecules were generated by chemically reacting more photoexcited carriers on the TiO_2 surface with H_2O and O_2 in the airflow. These photoexcited carriers originated from more oxygen-based species adsorbed and more oxygen vacancies introduced on the TiO_2 surface by the plasma-assisted-annealing.

Key words : Remote bactericidal effect / Anatase titanium dioxide nanoparticles / Plasma-assisted annealing / Reactive oxygen species / Hydrogen peroxide.

Superior technologies to control the spread of the coronavirus disease 2019 pandemic have been strongly desired (Khan et al., 2022; Prakash et al., 2022; Pasquale et al., 2021). The use of TiO_2-based photocatalytic semiconductors is one of the excellent technologies for pathogen disinfection (Khan et al., 2022; Prakash et al., 2022; Pasquale et al., 2021) and antibacterial applications (Singh et al., 2022; Liao et al., 2021; He et al., 2021a; He et al., 2021b; Liu et al., 2021). This reason is that TiO_2 irradiated with ultraviolet (UV) is more effective in eliciting microbial death than other photocatalytic semiconductors (Kubacka et al., 2014). The inactivation of bacteria due to TiO_2 is thought to be attributed to reactive oxygen species (ROS) generated by the TiO_2 surface under UV irradiation. Specifically, the electrons and holes photogenerated on the TiO_2 surface react chemically with O_2 and H_2O in the air to generate O_2^- and OH radicals, respectively (Arcanjo et al., 2018; Baniamerian et al., 2020; Wu et al., 2020). These ROS would attack the cell wall of bacteria adhering to the TiO_2 surface, damaging the cell membrane and destroying the cellular content (Dalrymple et al., 2010). Therefore, inactivating bacteria with TiO_2 requires bringing bacteria to the TiO_2 surface. For example, the bacterial inactivation of TiO_2 is performed by mixing bacterial suspensions with TiO_2 (Asahara et al., 2009), by dropping the bacterial suspensions onto the TiO_2 surface (Kawakami et al., 2021), and by carrying bacteria to the TiO_2 surface owing to air blowers and fan machines (Xu et al., 2019).

However, there is a crucial issue regarding the practical use of inactivating bacteria with TiO_2 photocatalysts. In contrast to ionic air purifiers in practice (Kivity et al., 2009; Hanond et al., 2011), TiO_2 photocatalysts hardly inactivate bacteria residing away from TiO_2. The

*Corresponding author. E-mail : retsuo(a)ee.tokushima-u.ac.jp

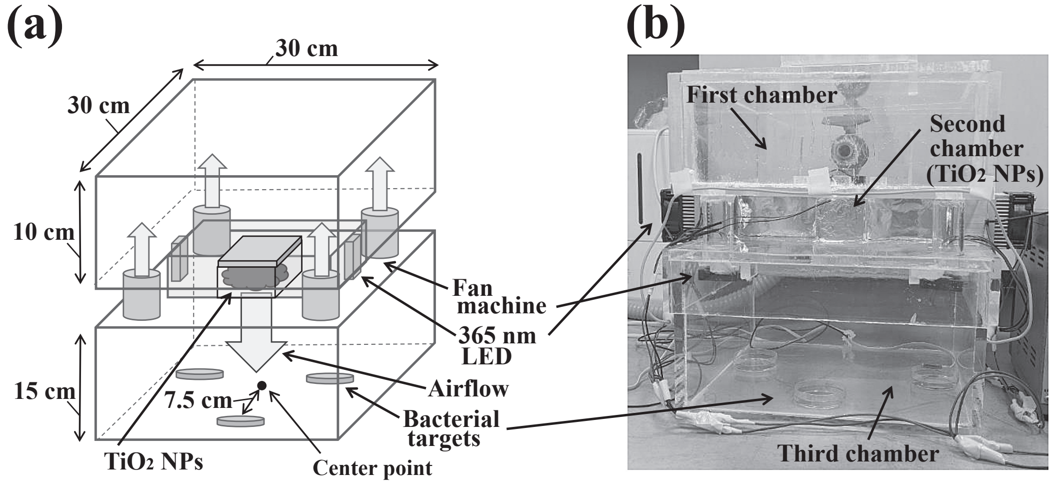

FIG. 1. (a) Schematic drawing and (b) photograph of a remote bactericidal device of TiO_2 NPs using a humid airflow. The developed device consists of three chambers made of transparent acrylic acid resin; from top to bottom, there are the first, second, and third chambers. Three bacterial targets were placed 7.5 cm away from the center point in the third chamber. The TiO_2 NPs immobilized on glass wool were set in the second chamber. The immobilized TiO_2 NPs were irradiated from two directions through a 1-cm think acrylic acid resin using two 365-nm UV LEDs. The humidified air was fed from a humidifier into the first chamber using tap water. A fan machine was used to force the humidified air in the first chamber into the third chamber through the immobilized TiO_2 NPs set in the second chamber. The humidified air reaching the third chamber was returned to the first chamber through four cylinders located near the four corners using four fan machines.

ionic air purifiers release cluster ions or radical ions into the air, inactivating bacteria present away from them or at distant places (Kivity et al., 2009; Hanond et al., 2011). In other words, the ionic air purifiers have remote bactericidal effects. Therefore, new technologies are required to achieve the remote bactericidal effect of TiO_2 photocatalysts.

In the present study, we have developed a remote bactericidal device of TiO_2 photocatalyst using a humidified airflow, as shown Fig. 1. This device was developed by referencing the literature on photocatalytic remote oxidation (Kubo et al., 2005 and 2006). That study revealed the oxidation effect at distant places but not the remote bactericidal effect (Kubo et al., 2005 and 2006). The TiO_2 photocatalyst used in the present study was anatase-type TiO_2 nanoparticles (NPs) annealed at 300℃ with a low-temperature O_2 plasma generated at atmospheric pressure (Kawakami et al., 2020a). The anatase-type TiO_2 NPs were TiO_2 NPs with an average size of 7 nm, called ST-01, purchased from Ishihara Sangyo, Japan. Employing the developed device, we investigated the remote bactericidal effect of plasma-assisted-annealed TiO_2 NPs. For comparison, anatase-type TiO_2 NPs annealed at 400℃ in ambient air (Kawakami et al., 2020a) were used. Herein, the remote bactericidal effect of plasma-assisted-annealed TiO_2 NPs is characterized by comparing it with those of the pristine TiO_2 NPs and air-annealed TiO_2 NPs. This remote bactericidal effect is also featured by comparing it with those of ionic air purifiers. The mechanism of remote bactericidal effect is discussed in terms of TiO_2-produced ROS in the humidified airflow. The present study emphasizes that the remote bactericidal device of anatase TiO_2 photocatalytic NPs developed is a valuable technology of inactivating bacteria at distant places.

The developed remote bactericidal device consists of three chambers made of transparent acrylic acid resin; as shown in Fig. 1, from top to bottom, there are the first, second, and third chambers. Three bacterial targets were placed 7.5 cm away from the center point in the third chamber with a volume of $30 \times 30 \times 15$ cm^3. The TiO_2 NPs immobilized on 9-μm diameter glass wool were set in the second chamber with a volume of $5 \times 5 \times 5$ cm^3. For this immobilization, the surface of glass wool 2 g in weight was irradiated for 3 min with an Ar plasma jet to enhance the wettability (Kawakami et al., 2020b). The Ar plasma jet was generated with a twisted wires-cylindrical electrode configuration (Kawakami et al., 2020b). After plasma irradiation, a 20-mL TiO_2 dispersion solution containing 0.66-g TiO_2 NPs was dripped onto the plasma-irradiated surface of glass wool. The dipped TiO_2 NPs were then allowed to dry naturally for three days to immobilize the TiO_2 NPs. The immobilized TiO_2 NPs were irradiated from two directions through a 1-cm think acrylic acid resin with an area of 5×5 cm^2

using two 365-nm ultraviolet (UV) light-emitting devices (LEDs) as shown in Fig. 1. The UV intensity at the immobilized TiO_2 NPs was 16.8 mW/cm^2 as measured with an optical power meter (Ophir Nova II). The humidified air was fed from a humidifier into the first chamber using tap water. The temperature and relative humidity (RH) in the chamber were the room temperature and 80%-95% RH, respectively. A fan machine was used to force the humidified air in the first chamber into the third chamber through the immobilized TiO_2 NPs set in the second chamber. The speed of airflow generated by the fan machine was 1.15 m/s as measured with an anemometer. The humidified air reaching the third chamber was returned to the first chamber through four cylinders, 2.4 cm in inner diameter and 5 cm long, located near the four corners using four fan machines as shown in Fig. 1. In other words, the humidified airflow was set to be circulated from the first chamber to the third chamber through the second chamber. The air circulation in the developed device, therefore, belongs to the internal air circulation.

The bacteria strain used were *Bacillus subtilis* (*B. subtilis*) American Type Culture Collection 6633 (Hassen et al., 2000). The bacterial cells were grown in Luria-Bertani (LB) broth (Nacalai Tesque Lennox, Japan) at 37℃ with shaking at 150 rpm for 17 h. The grown bacterial suspensions were centrifuged at 6,500 ×*g* for 3 min at 4℃ min to remove the LB broth and washed twice with sterile ion-exchanged water. The bacterial suspensions of 2×10^8 colony-forming units per mL (CFU/mL) were prepared in sterile ion-exchanged water. A 10 μL of the bacterial suspension was dropped onto a surface of 0.8% NaCl agar (SCA) in a dish 6 cm in diameter and 1.4 cm in height. The three bacteria-contained dishes were prepared and placed as the bacterial targets, as shown in Fig. 1. The remote bactericidal experiment was then performed for a time of 5 h. After the remote bactericidal experiment, each of the SCA surface was washed in a 1-mL solution of soybean-casein digest lecithin polysorbate (SCDLP) broth for 1 min to extract the bacteria from the SCA surface. A 0.1-mL broth suspension containing the bacteria was subjected to 10-fold serial dilutions using a 0.9-mL SCDLP broth. The serial dilutions plated on agar plates of SCDLP were incubated at 37℃ for 20 h. After incubation, the log numbers of bacterial colonies incubated on the agar plate were assessed using $|\log(N_t/N_0)|$, defined as the bactericidal level, where N_t and N_0 are the colony counts after and before the remote bactericidal experiment, respectively (Jang et al., 2016; Shi et al., 2019). The bactericidal level was measured three times for each TiO_2 sample set in the developed device. The measured data were analyzed statistically using the Tukey-Kramer test (Esumi Excel Tokei ver. 7.0, Japan). The results are presented as the averaged values with the standard deviations.

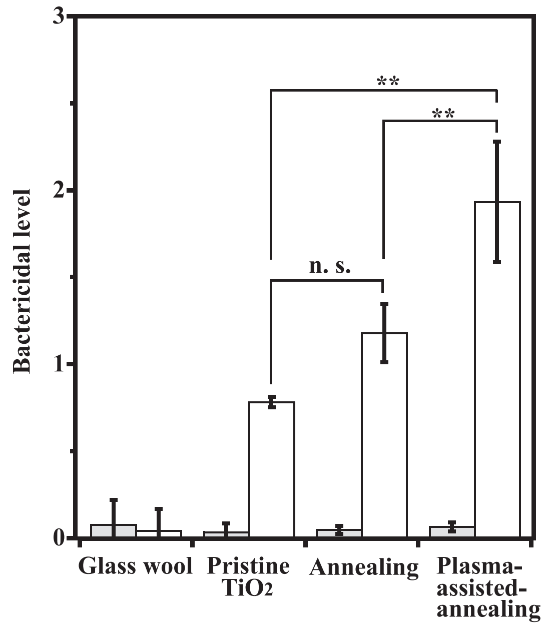

FIG. 2. Remote bactericidal effects of glass wool (without TiO_2 NPs), pristine TiO_2 NPs, air-annealed TiO_2 NPs, and plasma-assisted-annealed TiO_2 NPs in the presence (open bars) and absence (shaded bars) of UV irradiation. The symbol, **, corresponds to a *P* value < 0.01, as estimated by the Tukey-Kramer test. The abbreviation, n. s., signifies no significant differences, as estimated by the same test.

Figure 2 shows the remote bacterial effects of the TiO_2 samples set in the developed device. A high bactericidal level signifies a high remote bactericidal effect. The figure also shows the results obtained in the case of glass wool without TiO_2 NPs. In the case of glass wool without TiO_2 NPs, the bactericidal level is below 0.1 in the presence or absence of UV irradiation. This result indicates that the glass wool has no remote bactericidal effect. In the absence of UV irradiation, the bactericidal levels of any TiO_2 samples are below 0.1, indicating that the remote bactericidal effect of TiO_2 NPs does not work without UV irradiation. In contrast, the remote bactericidal effects of TiO_2 samples are exerted in the presence of UV irradiation. The bactericidal level of plasma-assisted-annealed TiO_2 NPs is approximately 2, suggesting a 99% viability reduction or 99% inactivation degree. The bactericidal level of air-annealed TiO_2 NPs, approximately 1, seems higher than that of pristine TiO_2 NPs, approximately 0.8, but there is no statistical difference between the two results. These values are half that of plasma-assisted-annealed TiO_2 NPs. The result suggests that the pristine TiO_2 NPs and air-annealed TiO_2 NPs have 88-90% inactivation degrees. Thus, the plasma-assisted-annealing contributes to increasing the remote bactericidal effect of TiO_2 NPs. On the other hand, the air-annealing does not increase the remote bactericidal effect.

The remote bactericidal effects obtained in the present study are compared with those induced by the ionic air purifiers or plasma cluster ion generators (Digel et al., 2005; Comini et al., 2021). Cluster ions generated with an ionic air purifier (Sharp Corp. Plasma Cluster, Japan) reduced the relative viable number of *B. subtilis* from 1.0 to 0.2 in 8 h (Digel et al., 2005). This result suggests that the inactivation degree of the generated cluster ions is 80%. Air ions generated with another ionic air purifier (Denso Thermal Systems Plasma Cluster Ionizer, Italy) inactivated 60% of *Escherichia coli* and 95% of *Staphylococcus aureus* in 8 h (Comini et al., 2021). These inactivation degrees are lower than that exerted by the remote bactericidal device of plasma-assisted-annealed TiO_2 NPs. These comparisons indicate that the developed remote bactericidal device with the plasma-assisted-annealed TiO_2 NPs is an effective means of inactivating bacteria at distant places.

The main factor of the remote bactericidal effect exerted by the plasma-assisted-annealed TiO_2 NPs would be the ROS traveled by the humidified airflow from the TiO_2 NPs. Since the distance from the TiO_2 NPs to the bacterial targets is approximately 16-20 cm and the humidified airflow speed is 1.15 m/s as describe above, the flight time of ROS traveled by the airflow to the bacterial target is estimated to be 140-173 ms. Considering the lifetimes of ROS (Zang et al., 1992; Hayyan et al., 2016), the lifetime of H_2O_2 molecules, 10^4 s (Zang et al., 1992), and the lifetime of O_2^- radicals, 1.25 s (Hayyan et al., 2016), are longer than the estimated flight time of ROS traveled by the airflow. According to the literature (Vernez et al., 2017), the ROS predominantly generated on anatase-type TiO_2 are H_2O_2 molecules, whereas O_2^- radicals are generated mainly on rutile-type TiO_2. Therefore, only H_2O_2 molecules in the humidified airflow would be allowed to reach the bacterial targets because the anatase-type TiO_2 NPs were used in the developed device. Figure 3 shows the concentrations of H_2O_2 molecules, which were generated by the pristine TiO_2 NPs and plasma-assisted-annealed TiO_2 NPs in a 5-h UV exposure and then traveled to the bacterial targets by the airflow in the remote bactericidal device. The H_2O_2 concentration was measured by the colorimetric method, i.e., the absorptiometry at a wavelength of 560 nm, based on the peroxide-mediated oxidation of Fe^{2+} followed by the reaction of Fe^{3+} with xylenol orange (Jiang et al., 1990; Shirai et al., 2022). The H_2O_2 measurement was performed three times for each TiO_2 sample under the same experimental conditions as those used for the remote bactericidal experiment. In the case of glass wool, the measured H_2O_2 concentration was 0.6-0.7 μM in the presence and absence of UV exposure (data not shown). The occurrence of this H_2O_2 concentration may be due to the presence of iron oxides such as $Fe(OH)_2$ contained in the humidified air produced from tap water because the glass wool does not inactivate the bacteria (Fig. 2). In the absorptiometry for H_2O_2, the presence of iron oxides may increase the absorbance, seemingly increasing the H_2O_2 concentration. Therefore, this increase is thought not to be a net increase in the H_2O_2 concentration. In the absence of UV exposure, the H_2O_2 concentration measured in each TiO_2 sample was similar to that observed for glass wool. The similarity suggests that the occurrence of this H_2O_2 concentration may originate from the presence of iron oxides in the humidified air because each TiO_2 sample in the absence of UV exposure does not inactivate the bacteria, as in the case of glass wool. As shown in Fig. 3, the H_2O_2 concentration of plasma-assisted-annealed TiO_2 NPs is approximately twice as high as that of pristine TiO_2 NPs. This higher H_2O_2 concentration would be attributed to the increased effective density of photoexcited carriers, which originates from more oxygen-based species adsorbed and more oxygen vacancies introduced on the TiO_2 surface by the plasma-assisted-annealing

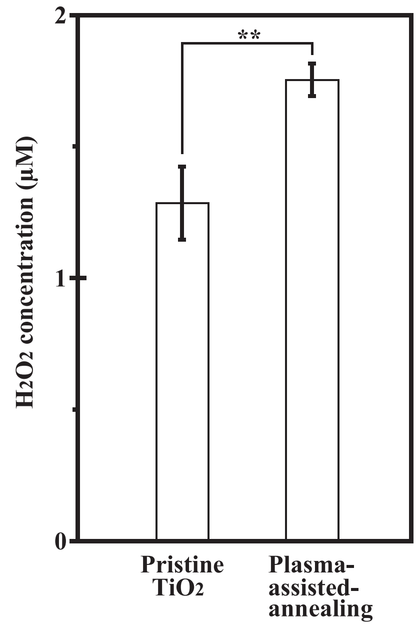

FIG. 3. Concentrations of H_2O_2 molecules, generated by pristine TiO_2 NPs and plasma-assisted-annealed TiO_2 NPs in a 5 h-UV exposure and then traveled to the bacterial targets in the remote bactericidal device. The two results have a significant difference of $^{**}P < 0.01$ as estimated by the two-tailed and unpaired t-test. The H_2O_2 concentration was measured three times for each TiO_2 sample.

(Kawakami et al., 2020a). The adsorbed oxygen-based species and introduced oxygen vacancies facilitate the charge separation by increasing the depletion layer width and trapping the photogenerated electrons, thus increasing the effective density of photoexcited carriers (Kawakami et al., 2020a). These photoexcited carriers would react chemically with H_2O and O_2 in the humidified airflow, thus generating more H_2O_2 molecules (He et al., 2021a). Specifically, more photogenerated holes react with H_2O in the humidified airflow, generating more OH radicals and H^+ ions. More photogenerated electrons react with O_2 in the airflow, generating more O_2^- radicals. The generated O_2^- radicals react with the generated H^+ ions to produce more HO_2 radicals. As a result, more H_2O_2 molecules are generated through 2 HO_2 radicals $\rightarrow H_2O_2 + O_2$. The H_2O_2 concentration result correlates with the remote bactericidal effect (Fig. 2). Thus, more H_2O_2 molecules traveled by the airflow would contribute primarily to the remote bactericidal effect of plasma-assisted-annealed TiO_2 NPs.

We have developed the remote bactericidal device of anatase TiO_2 photocatalytic NPs using the humidified airflow. Using this device, we clarified the remote bactericidal effect of plasma-assisted-annealed TiO_2 NPs by comparing it with those elicited by the pristine TiO_2 NPs and by the TiO_2 NPs annealed in ambient air. The plasma-assisted-annealed TiO_2 NPs significantly inactivated 99% of the bacterial cells in 5 h, whereas the pristine and air-annealed TiO_2 NPs inactivated 88-90% of the bacterial cells. This remote bactericidal effect was superior to those of the ionic air purifiers. The remote bactericidal effect of plasma-assisted-annealed TiO_2 NPs would be attributed to the larger amount of H_2O_2 molecules traveled by the humidified airflow from the TiO_2 NPs. These H_2O_2 molecules were generated through the chemical reactions of more photoexcited carriers on the TiO_2 surface with H_2O and O_2 in the humidified airflow. These photoexcited carriers originated from more oxygen-based species adsorbed and more oxygen vacancies introduced on the TiO_2 surface by the plasma-assisted-annealing. The findings obtained are vitally essential for fully understanding the remote bactericidal effect of photocatalysts. These findings will also provide a new perspective on photocatalytic applications for inactivating bacteria.

ACKNOWLEDGMENTS

Part of this work was supported by a regional revitalization grant utilizing local resources through industry-government-academia/department collaboration at Tokushima University and by JSPS KAKENHI Grant Number 20K03917.

CONFLICT OF INTEREST

The authors declare no conflict of interest.

REFERENCES

Arcanjo, G. S., Mounteer, A. H., Bellato, C. R., da Silva, L. M. M., Dias, S. H. B., and da Silva, P. R. (2018) Heterogeneous photocatalysis using TiO_2 modified with hydrotalcite and iron oxide under UV-visible irradiation for color and toxicity reduction in secondary textile mill effluent. *J. Environ. Manage*., **211**, 154-163.

Asahara, T., Koseki, H., Tsurumoto, T., Shiraishi, K., Shindo, H., Baba, K., Taoda, H., and Terasaki, N. (2009) The Bactericidal efficacy of a photocatalytic TiO_2 particle mixture with oxidizer against *Staphylococcus aureus*. *Jpn. J. Infect. Dis*., **62**, 378-380.

Baniamerian, H., Tsapekos, P., Morales, M. A., Shokrollahzadeh, S., Safavi, M., and Angelidaki, I. (2020) Effect of surfactants on photocatalytic toxicity of TiO_2-based nanoparticles toward *Vibrio fischeri* marine bacteria. *Inorg. Chem. Commun*., **116**, 107936:1-5.

Comini, S., Mandras, N., Iannantuoni, M. R., Menotti, F., Musumeci, A. G., Piersigilli, G., Allizond, V., Banche, G., and Cuffini, A. M. (2021) Positive and negative ions potently inhibit the viability of airborne Gram-positive and Gram-negative bacteria. *Microbiol. Spectr*., **9**, e00651-21:1-10.

Dalrymple, O. K., Stefanakos, E., Trotz, M. A., and Goswami, D. Y. (2010) A review of the mechanisms and modeling of photocatalytic disinfection. *Appl. Catal. B*, **98**, 27-38.

Digel, I., Artmann, A. T., Nishikawa, K., Cook, M., Kurulgan, E., and Artmann, G. M., (2005) Bactericidal effects of plasma-generated cluster ions. *Med. Biol. Eng. Comput*., **43**, 800-807.

Hanond, T., Chantarasuk, Y., Puangpan, S., Waropastrakul, N., Wongwajana, S., Sermswan, R. W., and Wongratanacheewin, S. (2011) Efficacy of ion generator against bacteria and fungi. *Srinagarind Med. J*., **26**, 301-308.

Hassen, A., Mahrouk, M., Quzari, H., Cherif, M., Boudabous, A., and Damelincourt, J. J. (2000) UV disinfection of treated wastewater in a large-scale pilot plant and inactivation of selected bacteria in a laboratory UV device. *Bioresour. Technol*., **74**, 141-150.

Hayyan, M., Hashim, M. A., and Alnashef, I. M. (2016) Superoxide ion: generation and chemical implications. *Chem. Rev*., **116**, 3029-3085.

He, J., Kumar, A., Khan, M., and Lo, I. M. C. (2021a) Critical review of photocatalytic disinfection of bacteria: from noble metals- and carbon nanomaterials-TiO_2 composites to challenges of water characteristics and strategic solutions. *Sci. Total Environ*., **758**, 143953:1-22.

He, J., Zheng, Z., and Lo, I. M. C. (2021b) Different responses of gram-negative and gram-positive bacteria to photocatalytic disinfection using solar-light-driven magnetic TiO_2-based material, and disinfection of real sewage. *Water Res*., **207**, 117816:1-10.

Jang, S. M, Sahastrabuddhe, S., Yun, C. H., Han, S. H., and Yang, J. S. (2016) Serum bactericidal assay for the evaluation of typhoid vaccine using a semi-automated colony-counting method. *Microb. Pathog*., **97**, 19-26.

Jiang, Z. Y., Woollard, A. C. S., and Wolff, S. P. (1990) Hydrogen peroxide production during experimental protein glycation. *FEBS*, **268**, 69-71.

Kawakami, R., Mimoto, Y., Yanagiya, S., Shirai, A., Niibe, M., Nakano, Y., and Mukai, T. (2021) Photocatalytic activity enhancement of anatase/rutile-mixed phase TiO_2 nanoparticles annealed with low-temperature O_2 plasma. *Phys. Status Solidi A*, **218**, 2100536:1-13.

Kawakami, R., Yoshitani, Y., Shirai, A., Yanagiya, S., Koide, H., Mimoto, Y., Kajikawa, K., Niibe, M., Nakano, Y., Azuma, C., and Mukai, T. (2020a) Effects of Nonequilibrium Atmospheric-Pressure O_2 Plasma-Assisted Annealing on Anatase TiO_2 Nanoparticles. *Appl. Surf. Sci*., **526**, 146684:1-12.

Kawakami, R., Yoshitani, Y., Mitani, K., Niibe, M., Nakano, Y., Azuma, C., and Mukai, T. (2020b) Effects of Air-Based Nonequilibrium Atmospheric Pressure Plasma Jet Treatment on Characteristics of Polypropylene Film Surfaces. *Appl. Surf. Sci*., **509**, 144910:1-10.

Khan, G. R., and Malik S. I. (2022) Ag-enriched TiO_2 nanocoating apposite for self-sanitizing/ self-sterilizing/ self-disinfecting of glass surfaces. *Mater. Chem. Phys*., **282**, 125803:1-10.

Kivity, S., Elbirt, D., Sade, K., Sthoeger, D., Sthoeger, Z., and Israeli Allergy Rhinitis/Asthma Study Group (2009) Efficacy of the Plasma Cluster device in asthmatic and/or allergic rhinitis patients with house dust mite allergy: a prospective observational pilot study. *Isr. Med. Assoc. J*., **12**, 74-77.

Kubacka, A., Diez, M. S., Rojo, D., Bargiela, R., Ciordia, S., Zapico, I., Albar, J. P., Barbas, C., dos Santos, V. A. P. M., García, M. F., and Ferrer, M. (2014) Understanding the antimicrobial mechanism of TiO_2-based nanocomposite films in a pathogenic bacterium. *Sci. Rep*., **4**, 4134:1-9.

Kubo, W., and Tatsuma, T. (2006) Mechanisms of photocatalytic remote oxidation. *J. Am. Chem. Soc*., **128**, 16034-16035.

Kubo, W., and Tatsuma, T. (2005) Photocatalytic remote oxidation with various photocatalyst and enhancement. *J. Mater. Chem*., **15**, 3104-3108.

Liao,Y., Zhou, Z., Dai, S., Jiang, L., Yang, P., Zhao, A., Lu, L., Chen, J., and Huang, N. (2021) Cell-friendly photo-functionalized TiO_2 nano-micro-honeycombs for selectively preventing bacteria and platelet adhesion. *Mater. Sci. Eng. C*, **123**, 111996:1-12.

Liu, N., Ming, J., Sharma, A., Sun, X., Kawazoe, N., Chen, G., and Yang, Y. (2021) Sustainable photocatalytic disinfection of four representative pathogenic bacteria isolated from real water environment by immobilized TiO_2-based composite and its mechanism. *Chem. Eng. Sci*., **426**, 131217:1-12.

Pasquale, I. D., Porto, C. L., Edera, M. D., Curri, M. L., and Comparelli, R. (2021) TiO_2-based nanomaterials assisted photocatalytic treatment for virus inactivation: perspectives and applications. *Curr. Opin. Chem. Eng*., **24**, 100716:1-10.

Prakash, J., Cho, J., and Mishra, Y. K. (2022) Photocatalytic TiO_2 nanomaterials as potential antimicrobial and antiviral agents: Scope against blocking the SARS-COV-2 spread. *Micro Nano Eng*., **14**, 100100:1-16.

Shi, J., Zhang, F., Wu, S., Guo, Z., Huang, X., Hu, X., Holmes, M., and Zou, X. (2019) Noise-free microbial colony counting method based on hyperspectral features of agar plates. *Food Chem*., **274**, 925-932.

Shirai A, Kawasaka K., and Tsuchiya K. (2022) Antimicrobial action of phenolic acids combined with violet 405-nm light for disinfecting pathogenic and spoilage fungi. *J. Photochem. Photobiol. B*, **229**, 112411.

Singh, T., Pal, D. B., Almalki, A. H., Althobaiti, Y. S., Alkhanani, M. F., Haque, S., Sharma, S., and Strivastava, N. (2022) Green synthesis of TiO_2 bionanocomposite using waste leaves of water hyacinth. *Mater. Lett*., **316**, 132012:1-3.

Vernez, D., Sauvain, J. J., Laulagnet, A., Otano, A. P., Hopf, N. B., Batsungnoen, K., and Suarez, G. (2017) Airborne nano-TiO_2 particles: an innate or environmentally-induced toxicity?. *J. Photochem. Photobiol. A: Chem*., **343**, 119-125.

Wu, X., Cao, L., Song, J., Si, Y., Yu, J., and Ding, B. (2020) Thorn-like $Ag_2C_2O_4/TiO_2$ nanofibers as hierarchical heterojunction photocatalysts for efficient visible-light-driven bacteria-killing. *J. Colloid Interface Sci*., **560**, 681-689.

Xu, S., Lu, W., Chen, S., Xu, Z., Xu, T., Sharma, V. K., and Chen, W. (2019) Colored TiO_2 composites embedded on fabrics as photocatalysts: decontamination of formaldehyde and deactivation of bacteria in water and air. *Chem. Eng. J*., **375**, 121949:1-10.

Zang, L. Y., and Misra, H. P. (1992) EPR Kinetic Studies of Superoxide Radicals Generated during the Autoxidation of l-Methyl-4-phenyl-2,3-dihydropyridinium, a Bioactivated Intermediate of Parkinsonian-inducing Neurotoxin l-Methyl-4-phenyl-l,2,3,6-tetrahydropyridine. *J. Biol. Chem*., **267**, 23601-23608.